Available online at www.sciencedirect.com

ScienceDirect

Procedia CIRP 105 (2022) 278–283

www.elsevier.com/locate/procedia

29th CIRP Life Cycle Engineering Conference

Assessing the efficiency of Laser-Induced Breakdown Spectroscopy (LIBS) based sorting of post-consumer aluminium scrap

Simon Van den Eynde[a]*, Dillam Jossue Diaz-Romero[a,b], Bart Engelen[a,c], Isiah Zaplana[a], Jef R. Peeters[a]

[a]*Department of Mechanical Engineering – KU Leuven, Celestijnenlaan 300A, Box 2422, 3001, Leuven, Belgium*
[b]*PSI-EAVISE – KU Leuven, Jan Pieter De Nayerlaan 5, 2860, Sint-Katelijne-Waver, Belgium*
[c]*Technology Campus Diepenbeek – KU Leuven, Agoralaan Gebouw B, 3590, Diepenbeek, Belgium*

* Corresponding author. Tel.: +32 499 167 489. *E-mail address:* simon.vandeneynde@kuleuven.be

Abstract

The aluminium Twitch fraction of a Belgian recycling facility could be further sorted by implementing Laser-Induced Breakdown Spectroscopy (LIBS). To achieve this goal, the presented research identifies commercially interesting output fractions and investigates machine learning methods to classify the post-consumer aluminium scrap samples based on the spectral data collected by the LIBS sensor for 834 aluminium scrap pieces. The classification performance is assessed with X-Ray Fluorescence (XRF) reference measurements of the investigated aluminium samples, and expressed in terms of accuracy, precision, recall, and f1 score. Finally, the influence of misclassifications on the composition of the desired output fractions is evaluated.

Keywords: Aluminium, Post-consumer scrap; Sorting; Laser-Induced Breakdown Spectroscopy; Classification

1. Introduction

The European Aluminium Association (EAA) aims to increase the amount of secondary aluminium in European end-use products from 26% in the year 2000 to 49% in 2050 [1]. One prominent strategy to achieve this goal is to improve state-of-the-art sorting methods [2]. One of the most promising technologies that is being developed to separate different aluminium alloys is Laser-Induced Breakdown Spectroscopy (LIBS) [3,4]. This technology uses laser pulses to ablate the surface of the investigated material so that plasma is formed where the pulses hit the surface, and light is emitted. A spectrometer converts the detected light into a spectrum characteristic for the material subjected to the LIBS analysis. Sorting post-consumer aluminium scrap can be interesting for recycling companies because aluminium with lower concentrations of alloying elements can be sold at a higher price due to its broader applicability compared to mixed aluminium scrap. Therefore, this research investigates the opportunities of LIBS based aluminium sorting for a large scale Belgian recycling facility to increase the value of the collected post-consumer aluminium scrap.

2. Methodology

2.1. Selection of sorting targets

The output fraction of the aluminium recycling facility in this case study is a mix of post-consumer aluminium scrap containing wrought and cast alloys from products of different sectors. The dimensions of the shredded aluminium pieces are between 40 and 120 mm as a result of two sieving steps. This output fraction, called "Twitch", is only to a very limited extent contaminated with materials other than aluminium [5].

10.1016/j.procir.2022.02.046

However, due to the presence of multiple different aluminium alloys, the fraction can today only be sold to refiners to produce cast alloys. Since there is a wide variety in the composition of the scrap pieces in this fraction, enhanced sorting could yield additional financial benefits if valuable sorting targets can be selected and separated.

The selection of the sorting targets of the LIBS sorting step in this case study is based on discussions with the involved recycling company and based on the current demand for secondary aluminium. The first of the three selected target fractions is the "Premium" class. This class has severe limits to the concentrations of the most common alloying elements. Its purpose is to be sold at a significantly higher price than the current output fraction to refiners to dilute low purity scrap for the production of cast alloys or to remelters for the production of secondary wrought alloys. The second class is called "Desox". It stands for "deoxidation aluminium" which, according to the EAA definition, is aluminium consisting of alloys with a high concentration of metallic aluminium (usually exceeding 95%) used to remove free oxygen from liquid steel [6]. The last target fraction is the "Secondary" class. This fraction is meant to be sold to refiners at a similar price as the current output fraction for the production of cast alloys. Therefore, it must still meet the refiners' composition requirements. Table 1 shows the allowable concentration of each alloying element in the different target classes.

Table 1: Limit values for concentrations of alloying elements in the desired output fractions

Element	Premium	Desox	Secondary
Al		>95%	
Cu	<0,04 wt%	<2 wt%	<3,3 wt%
Zn	<0,05 wt%	<1 wt%	<1,2 wt%
Fe	<0,25 wt%	<0,4 wt%	<0,6 wt%
Mn	<0,06 wt%	<1 wt%	<0,4 wt%
Mg	<0,40 wt%	<1 wt%	<0,45 wt%
Si	<0,50 wt%	<2 wt%	<9,4 wt%
Ni		<1 wt%	<0,3 wt%
Cr		<1 wt%	
Sn		<2 wt%	<0,1 wt%
Ti		<1 wt%	<0,1 wt%
Sr			<0,05 wt%
Pb			<0,2 wt%

2.2. Sampling and Measuring procedure

A representative sample of the existing output fraction, consisting of 834 pieces weighing 39.28 kg in total, has been acquired and analysed with the following sampling and measuring procedure, illustrated in Figure 1 with capital letters that correspond to the different steps. The Twitch fraction, from which the sample is collected, is stored at the site of the recycling facility (A). Nine zones are delimited in the stored Twitch fraction (B). From each zone, an amount of aluminium is collected with a crane to ensure that the sample's representativeness would not be degraded due to inhomogeneity of the material across the different zones (C). Afterwards, the collected pieces from the different zones are mixed, spread and divided into four different equal-looking subsamples (D). One subsample is selected as the dataset for the analysis in this research (E).

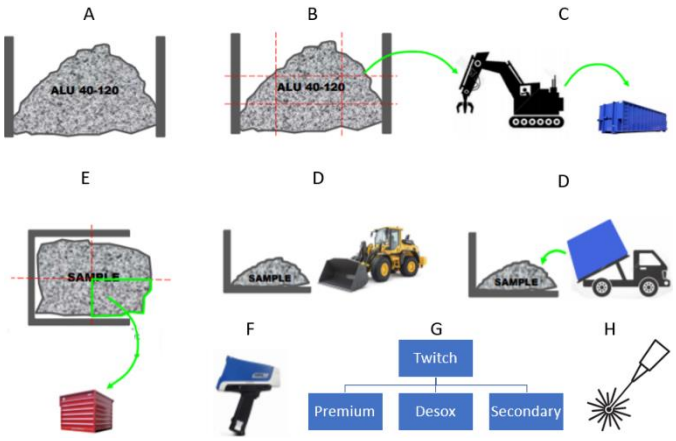

Figure 1: Graphical representation of sampling and measuring procedure

Subsequently, each metal piece in the acquired dataset has been labelled with a unique number. Then, a part of the piece's surface has been cleaned with a Dremel and ethanol, after which the composition of each piece is measured by performing an XRF analysis on the cleaned part of the piece (F). For this analysis, an Olympus Vanta handheld XRF analyser is used. Based on the results of the XRF analysis and the concentration limits for the desired fractions, shown in Table 1, every piece in the dataset is assigned to one of the target classes (G). Therefore, the "ground truth" classification in this research relies on the performance of the XRF. When assigning the pieces to the ground truth classes, only the alloying elements are considered that are most critical to this case study, namely copper, zinc, silicon, and manganese. Only these elements are considered for the class assignment, because the value of the output fraction does not significantly decrease when the concentrations of the less critical elements slightly exceed the specified limits.

Furthermore, it is expected that the concentrations of the less critical elements will average out to a level around or below the specified limits. When only considering the most critical elements to assign the pieces to the ground truth classes, it can be avoided that pieces are unnecessarily excluded from the more valuable Premium and Desox classes due to one or a few less critical alloy concentrations that exceed the specified limits in Table 1. All pieces that do not meet the conditions of the Premium or Desox class are assigned to the Secondary class, even when the restrictions for the Secondary class are not met. This approach is adopted instead of defining a fourth class of pieces because this research aims to assess the feasibility of a three-way sorting system based on LIBS classification. This way, the Premium, Desox, and Secondary classes constitute 28.3%, 28.8%, and 42.9% of the mass of the total sample, respectively.

Next, the LIBS experiment is conducted (H). The custom made LIBS system in this research is a gated LIBS. The laser has a pulse energy of 80 mJ and is fired at a frequency of 10 Hz. A CMOS camera (1936 x 1216 pixels) detects the light emitted from the ablated surface. The Echelle type spectrometer of the system has a spectral range between 180 nm and 800 nm and a spectral resolution that goes from 0.15

nm at 180 nm wavelength up to 0.4 nm at 800 nm wavelength. The exposure time is 85 µs. For each piece in the dataset, two LIBS measurements are conducted: one on the cleaned part of the piece's surface and one on an uncleaned part of the surface. The pieces are placed in a fixed position for the measurements, at 300 mm in front of the LIBS outer lens, in focus of the laser. The position is controlled with a distance sensor with a 0.1 mm resolution. When appropriately positioned, with the surface of the piece perpendicular to the trajectory of the laser, ten laser pulses are fired, and ten spectra are collected for each measurement.

2.3. Signal Pre-processing

Prior to classification, the spectra are pre-processed to enhance the performance of the classifying algorithms. A first problem that necessitates pre-processing is that the recorded LIBS signals are a superposition of the emission signal of the analyte, the emission signal due to plasma continuum, and the detector-associated signal [7]. The analyte signal corresponds to the detected radiation emitted by the alloying elements of interest at specific atomic or ionic transitions. This part of the signal is characteristic for the material's composition and can be used to classify the aluminium pieces. The plasma continuum signal, also referred to as the continuum background, is composed of recombination emission and bremsstrahlung from free electrons [8]. The detector-associated signal is usually caused by the dark current of the detector or stray light. A typical solution for this problem, which is applied in this research, is baseline correction. This method removes the continuum background and detector-associated signal from the recorded spectra [9,10]. The applied baseline removal method is based on the asymmetric least squares smoothing approach suggested by Eilers and Boelens [11].

A second pre-processing step is the removal of recorded intensities that relate to saturated pixels. This step is conducted because once a pixel is saturated, it no longer captures the physical relation between the intensity of the recorded radiation and the concentration of the alloying elements. The removed intensity values are replaced by interpolating the adjacent values. From the ten spectra that are collected per measurement, only the one is used with the highest signal-to-noise ratio. The mentioned pre-processing steps are applied to that spectrum.

2.4. Feature Extraction

After pre-processing, three types of features are extracted from the LIBS spectra to reduce the number of variables involved in the classification task and to decrease as such the computational burden. Furthermore, feature extraction mitigates the risk of overfitting in classification tasks [12].

The first type is a set of 70 handcrafted features that includes several spectral descriptors and other metrics typically extracted as features in sound description research, speech recognition research, and other scientific fields. The spectral descriptors extracted as features are spectral flux, spectral centroid, spectral crest, spectral flatness, spectral kurtosis, spectral entropy, spectral bandwidth, and spectral skewness [13,14]. The other handcrafted features are the peak frequency, the power of the spectrum, the Mean Instantaneous Frequency (MIF) [15], the Mean Instantaneous Bandwidth (MIB) [15], Long-Term Average Spectrum (LTAS) [16], Envelope Modulation Spectrum (EMS) [16], Octave-based Modulation Spectral Contrast (OMSC) [17], Linear Spectral Frequency (LSF) [18], Time-Frequency Representation (TFR) [19], chroma features [20], features extracted through Linear Predictive Coding (LPC) [18,21,22] and features extracted through the Method of Selection of Amplitudes of Frequency Multi-expanded Filter developed by Glowacz et al. [23,24]. The second type of extracted features is a set of 11 "peak features" that hold information on the (relative) intensities of the most prominent peaks in the recorded spectra. Finally, the third type of features corresponds to the maximum intensity values in 136 selected regions of interest (ROI). Since the atomic and ionic transitions of relevant alloying elements emit radiation at specific wavelengths, the intensities of the recorded spectra at these wavelengths are expected to be the most critical for classification. The ROI are defined as 1 nm wavelength ranges around the wavelengths that, according to the NIST LIBS database, correspond to the atomic and ionic transitions of the alloying elements considered in this research [25].

2.5. Classification

Various classification algorithms, such as Random Forest (RF) [26], Support Vector Machine (SVM) [27,28] and Logistic Regression (LR) [29], have been investigated in recent research to distinguish metals based on LIBS spectra. These three methods are implemented in this research to classify the aluminium pieces in the desired categories. Three cases are investigated. In the first case, the classifier algorithms are trained and tested with the LIBS spectra collected when shooting on the cleaned surface of the aluminium pieces. In the second case, the classifiers are trained and tested with spectra corresponding to the uncleaned part of the surface. In the third case, both the clean and unclean spectra are used for training and testing. These three cases are investigated and compared since the surface condition is suspected to have a significant impact on the classification performance.

The performance of these methods is expressed with four metrics: accuracy, weighted average precision, weighted average recall, and weighted average f1 score. Accuracy is the percentage of correctly classified pieces. Precision (P) is the ratio between the number of true positives (T_p) and the sum of the numbers of true positives and false positives (F_p). Recall (R) is the ratio between the number of true positives and the sum of the numbers of true positives and false negatives (F_n). The f1 score is the harmonic mean of precision and recall (see Formula 1). 20% of the dataset is used as a test set to evaluate the performance. The results of the three cases are compared to assess the influence of the surface condition of the samples on the classification performance.

$$P = \frac{T_p}{T_p+F_p} \qquad R = \frac{T_p}{T_p+F_n} \qquad f1 = 2\frac{P*R}{P+R} \tag{1}$$

The impact of misclassifications on the composition of the desired output fractions is assessed as well. First, the

composition is calculated for each of the three desired classes when every piece in the dataset is assigned to its ground truth class, based on the weight and measured composition of each piece. Afterwards, the composition of the three fractions is computed when the aluminium pieces are classified relying on the best performing classification algorithm. This is demonstrated for the three different surface conditions.

3. Results

Table 2 shows the performance metrics for the three classifiers in the three surface conditions (metrics for best performing classifier per surface condition in bold). With an accuracy of 65.82%, the classification performance for the clean surface condition of the Random Forest algorithm is slightly better than that of the SVM classifier (65.19%) and the Logistic Regression classifier (61.39%). The other metrics are close to the accuracy score and indicate the same ranking between the classifiers.

Table 2: Performance metrics for the different classifiers and surface conditions

Classifier	Metric	Clean	Unclean	Both
Logistic Regression	Accuracy	61.39%	55.10%	62.54%
	Precision	0.609	0.560	0.621
	Recall	0.614	0.551	0.625
	f1 score	0.603	0.525	0.606
Support Vector Machine	Accuracy	65.19%	**60.76%**	**62.86%**
	Precision	0.656	**0.608**	**0.624**
	Recall	0.652	**0.607**	**0.629**
	f1 score	0.637	**0.579**	**0.624**
Random Forest	Accuracy	**65.82%**	59.49%	62.54%
	Precision	**0.667**	0.583	0.620
	Recall	**0.658**	0.595	0.625
	f1 score	**0.645**	0.585	0.622

For the uncleaned surface condition, the classification accuracy is slightly worse: the SVM classifier (60.76%) outperforms the RF (59.49%) and LR (55.10%) classifiers. In the third case, where the spectra of both the cleaned and uncleaned surfaces are used for training and testing, the performance metrics are situated in between those of the two previous cases. The SVM classifier (62.86% accuracy) again outperforms the RF (62.54%) and LR (62.54%) classifiers.

Table 3 shows the composition of the three desired output fractions when all pieces in the dataset are assigned to the three classes according to the ground truth labels. The concentrations of the elements are expressed in weight percent (wt%). As a result of the chosen approach to assign the ground truth labels, some less critical elements narrowly exceed the specified concentration limits for the desired output fractions (marked in orange). The iron content is slightly higher than desired in each output fraction, as well as the magnesium content in the Desox class. However, all other considered alloying elements, including the most critical elements, meet the specified restrictions with a significant margin.

Table 3: Composition of desired output fractions when separated according to ground truth measurements and specified concentration tolerances (concentrations in wt%)

Element	Premium	Desox	Secondary
Al	99.239	97.622	88.345
Cu	0.005	0.170	1.978
Zn	0.010	0.042	0.907
Fe	0.259	0.421	0.812
Mn	0.013	0.288	0.293
Mg	0.259	1.096	0.150
Si	0.187	0.236	7.178
Ni	0.003	0.029	0.045
Cr	<0.001	0.031	0.021
Sn	<0.001	<0.001	0.013
Ti	0.006	0.036	0.042
Sr	<0.001	<0.001	0.004
Pb	0.002	0.009	0.180

Table 4 shows the composition of the output fractions when the aluminium pieces in the test set are classified using the Random Forest algorithm, relying on the spectra collected in the clean surface condition. Mainly due to Secondary pieces that are classified as Premium pieces, the zinc concentration of the Premium fraction exceeds the specified limit of 0.05 wt% (marked in red). This is the most detrimental effect of the misclassifications since all other concentrations are still below the specified limits, except for the magnesium content in the Desox fraction, which is just higher than the specified limit. Another adverse effect of the misclassifications is that a significant amount of Premium and Desox pieces end up in a less valuable fraction. The misclassifications cause the aluminium concentrations in the three output fractions to lie significantly closer to each other than in the ground truth case because of the diluting effect of the very pure Premium pieces in the lower classes. So, while the negative effect of the misclassifications on the composition of the Premium and Desox class is moderate, the fact that many purer pieces do not end up in the more valuable fractions defeats in part the purpose and the benefit of the LIBS classification.

Table 4: Composition of desired output fractions when classified with Random Forest for the clean surface condition (concentrations in wt%)

Element	Premium	Desox	Secondary
Al	99.136	97.798	93.866
Cu	0.009	0.052	0.931
Zn	0.180	0.047	0.537
Fe	0.240	0.320	0.544
Mn	0.017	0.272	0.260
Mg	0.197	1.037	0.166
Si	0.190	0.411	3.509

Ni	0.003	0.004	0.081
Cr	0.001	0.020	0.019
Sn	<0.001	<0.001	0.007
Ti	0.004	0.003	0.012
Sr	<0.001	<0.001	0.001
Pb	0.004	0.015	0.039

Table 5 shows the composition of the output fractions when the aluminium pieces in the test set are classified using the SVM algorithm, relying on the spectra collected in the uncleaned surface condition. For the uncleaned surface condition, the composition of the Premium class is more severely affected by the misclassifications. Now, the concentration limits of both copper and manganese are exceeded (marked in red), as well as those of the less critical elements iron and magnesium (marked in orange). The compositions of the Desox and Secondary fractions do meet the specified restrictions. Due to the diluting effect of misclassified Premium and Desox pieces, the aluminium concentrations of the three fractions are much closer together than in the ground truth case. The aluminium concentration of the Desox fraction is now even slightly higher than that of the Premium class, mainly since the magnesium concentration in the Premium class is relatively high.

Table 5: Composition of desired output fractions when classified with SVM for the uncleaned surface condition (concentrations in wt%)

Element	Premium	Desox	Secondary
Al	97.975	98.400	94.054
Cu	0.079	0.125	0.860
Zn	0.023	0.054	0.564
Fe	0.358	0.299	0.521
Mn	0.134	0.075	0.293
Mg	0.957	0.271	0.308
Si	0.281	0.740	3.228
Ni	0.004	0.007	0.078
Cr	0.032	0.009	0.018
Sn	<0.001	0.001	0.006
Ti	0.005	0.006	0.011
Sr	<0.001	<0.001	0.001
Pb	0.078	0.004	0.033

Table 6 shows the composition of the output fractions in the case where both surface conditions are combined for training and testing, when the pieces are classified with the SVM classifier. While the classification accuracy for this case is higher than for the uncleaned surface condition, more Secondary pieces end up in the Premium class, resulting in alloying concentrations in the Premium class that exceed the specified limits for all critical elements and iron. Some less critical elements also exceed the limits in the Desox and Secondary fraction.

Table 6: Composition of desired output fractions when classified with SVM for the clean and uncleaned surface condition (concentrations in wt%)

Element	Premium	Desox	Secondary
Al	97.228	96.856	90.099
Cu	0.186	0.136	2.690
Zn	0.106	0.293	0.830
Fe	0.346	0.310	0.826
Mn	0.125	0.280	0.289
Mg	0.377	1.612	0.240
Si	1.580	0.438	4.543
Ni	0.009	0.005	0.040
Cr	0.007	0.032	0.023
Sn	0.002	0.000	0.015
Ti	0.015	0.007	0.052
Sr	0.002	0.001	0.001
Pb	0.010	0.010	0.326

4. Discussion

While the accuracy of the different classifiers is not exceptionally high, the resulting compositions of the output fractions are still promising, especially for the clean surface condition. This is because most of the misclassified pieces have a composition that is on the edge of either the Premium and Desox class or the Desox class and the Secondary class. Therefore, misclassifying such pieces has no devastating impact on the composition of the fraction where these pieces end up. The most critical misclassifications are those that assign Secondary pieces to the Premium fraction, and elevate the concentrations of the most critical alloying elements.

Another issue that limits the achievable performance of the classifiers is that the XRF measurements also are not perfectly reliable, especially for lighter elements such as silicon and magnesium. Mainly for pieces on the edge between two classes, the ground truth class assignment might be wrong due to measurement inaccuracies, causing confusion while training. The classifiers trained on this ground truth are therefore limited in their performance by that of the XRF.

Also the presence of leftover surface contamination, even after cleaning, can influence the composition measurements, especially for iron. Ferrosilicon powder particles used to make the suspension in density separation processes, remain on the surface and increase the measured iron concentration.

5. Conclusion and future work

This research presented a novel method for evaluating spectroscopic sorting systems for metal recycling and shows that the use of classification algorithms on LIBS spectra is highly promising for post-consumer scrap. Random Forest is the best performing classifier for the clean surface condition, while the SVM classifier performs best for the other two cases. The spectra collected from clean surfaces yield the best results. Combining spectra form clean and uncleaned surfaces slightly improves the classification accuracy, but not the composition

of the output fractions. While the accuracy of the classifiers is rather limited, the presented results demonstrate that the thresholds on the desired output fractions are almost reached. Considering that the separation of aluminium alloys in mixed post-consumer scrap is notoriously difficult due to the variety in the composition and the surface contamination on the pieces, this is a valuable conclusion. In future work, a better method to find a ground truth must be adopted. Cross-validating the ground truth classes with multiple composition measurement techniques will be explored. The used classifying methods and the feature extraction method must be optimised. Additional physically meaningful hand-crafted features will be introduced. Finally, a thorough economic analysis will be performed.

Acknowledgements

This work has received funding from the European Institute of Innovation and Technology (EIT), a body of the European Union, under the Horizon 2020, the EU Framework Programme for Research and Innovation in the AUtomatic SOrting of mixed scrap Metals (AUSOM) project (project number 19294, https://www.ausomproject.eu/).

References

[1] European Aluminium Association. VISION 2050: European Aluminium's Contribution to the EU's Mid-Century Low-Carbon Roadmap. 2019. [Online]. Available: https://www.european-aluminium.eu/media/2552/sample_executive-summary-vision-2050_web_pages_20190408.pdf

[2] Simon Van den Eynde, Ellen Bracquené, Dillam Diaz-Romero, Isiah Zaplana, Bart Engelen, Joost R. Duflou, Jef R. Peeters. Forecasting global aluminium flows to demonstrate the need for improved sorting and recycling methods. Waste Management 2022;137:231-240. doi: 10.1016/j.wasman.2021.11.019

[3] Campanella B, Grifoni E, Legnaioli S, Lorenzetti G, Pagnotta S, Sorrentino F, Palleschi V. Classification of wrought aluminum alloys by Artificial Neural Networks evaluation of Laser Induced Breakdown Spectroscopy spectra from aluminum scrap samples. Spectrochimica Acta Part B: Atomic Spectroscopy 2017;134:52-57. doi: 10.1016/j.sab.2017.06.003.

[4] He X, Dong B, Chen Y, Li R, Wang F, Li J, Cai Z. Analysis of magnesium and copper in aluminum alloys with high repetition rate laser-ablation spark-induced breakdown spectroscopy. Spectrochimica Acta Part B: Atomic Spectroscopy 2018;141:34-43. doi: 10.1016/j.sab.2018.01.007.

[5] Soo VK, Peeters J, Paraskevas D, Compston P, Doolan M, Duflou JR. Sustainable aluminium recycling of end-of-life products: A joining techniques perspective. Journal of Cleaner Production 2018;178:119-132. doi: 10.1016/j.jclepro.2017.12.235.

[6] European Aluminium Association. Ea Recycling Brochure 2016. European Aluminium Association 2016. Accessed: Sep. 03, 2021. [Online]. Available: https://european-aluminium.eu/media/1712/ea_recycling-brochure-2016.pdf

[7] Hahn DW, Omenetto N. Laser-Induced Breakdown Spectroscopy (LIBS), Part II: Review of Instrumental and Methodological Approaches to Material Analysis and Applications to Different Fields. Applied Spectroscopy 2012;66:347-419.

[8] Tognoni E, Cristoforetti G. Signal and noise in Laser Induced Breakdown Spectroscopy: An introductory review. Optics & Laser Technology 2016;79:164-172. doi: 10.1016/j.optlastec.2015.12.010.

[9] Schröder S, Meslin PY, Gasnault O, Cousin A, Maurice S, Lasue J, Forni O, Wiens RC, MSL Science Team. ChemCam's dark spectra and their role in the detection of hydrogen in the LIBS data. 45th Lunar and Planetary Science Conference 2014.

[10] Yaroshchyk P, Eberhardt JE. Automatic correction of continuum background in Laser-induced Breakdown Spectroscopy using a model-free algorithm. Spectrochimica Acta Part B: Atomic Spectroscopy 2014;99:138-149. doi: 10.1016/j.sab.2014.06.020.

[11] Eilers PHC, Boelens HFM. Baseline correction with asymmetric least squares smoothing. Leiden University Medical Centre Report 2005;1

[12] Liu R, Gillies DF. Overfitting in linear feature extraction for classificationof high-dimensional image data. Pattern Recognition 2016;53:73-86. doi: 10.1016/j.patcog.2015.11.015.

[13] Peeters G. A large set of audio features for sound description (similarity and classification) in the CUIDADO project. Ircam, Paris, France, 2004. [Online]. Available: https://www.yumpu.com/es/document/read/11364288/a-large-set-of-audio-features-for-sound-description-www-ircam/15

[14] Chiang S, Vankov ER, Yeh HJ, Guindani M, Vannucci M, Haneef Z, Stern JM. Temporal and spectral characteristics of dynamic functional connectivity between resting-state networks reveal information beyond static connectivity. PLoS ONE 2018;13. doi: 10.1371/journal.pone.0190220.

[15] Jones G, Boashash B. Instantaneous frequency, instantaneous bandwidth and the analysis of multicomponent signals. Acoustics, Speech, and Signal Processing 1988: 2467-2470. doi: 10.1109/ICASSP.1990.116092.

[16] Fletcher AR, Wisler AA, McAuliffe MJ, Lansford KL, Liss JM. Predicting Intelligibility Gains in Dysarthria Through Automated Speech Feature Analysis. Journal of Speech, Language, and Hearing Research 2017;60:3058-3068. doi: 10.1044/2017_JSLHR-S-16-0453.

[17] Lee C, Shih J, Yu K, Su J. Automatic Music Genre Classification using Modulation Spectral Contrast Feature. IEEE International Conference on Multimedia and Expo 2007. doi: 10.1109/ICME.2007.4284622.

[18] Kabal P, Ramachandran RP. The Computation of Line Spectral Frequencies Using Chebyshev Polynomials. IEEE Transactions on Acoustics, Speech, and Signal Processing 1986;34:1419-1426.

[19] Portnoff M. Time-frequency representation of digital signals and systems based on short-time Fourier analysis. IEEE Transactions on Acoustics, Speech, and Signal Processing 1980;28:55-69. doi: 10.1109/TASSP.1980.1163359.

[20] Maršík L, Rusek M, Slaninová K, Martinovič J, Pokorný J. Evaluation of Chord and Chroma Features and Dynamic Time Warping Scores on Cover Song Identification Task. Computer Information Systems and Industrial Management 2017:205-217. doi: 10.1007/978-3-319-59105-6_18.

[21] Anjum MF, Dasgupta S, Mudumbai R, Singh A, Cavanagh JF, Narayanan NS. Linear predictive coding distinguishes spectral EEG features of Parkinson's disease. Parkinsonism & Related Disorders 2020;79:79-85. doi: 10.1016/j.parkreldis.2020.08.001.

[22] Hanson HM, Maragos P, Potamianos A. A system for finding speech formants and modulations via energy separation. IEEE Transactions on Speech and Audio Processing 1994;2:436-443.

[23] Glowacz A, Glowacz W, Glowacz Z, Kozik J. Early fault diagnosis of bearing and stator faults of the single-phase induction motor using acoustic signals. Measurement 2018;113:1-9. doi: 10.1016/j.measurement.2017.08.036.

[24] Glowacz A. Fault Detection of Electric Impact Drills and Coffee Grinders Using Acoustic Signals. Sensors 2019;19. doi: 10.3390/s19020269.

[25] Kramida A, Olsen K, Ralchenko Y. NIST LIBS Database. [Online]. Available: https://physics.nist.gov/PhysRefData/ASD/LIBS/libs-form.html

[26] Zhan L, Ma X, Fang W, Wang R, Liu Z, Song Y, Zhao H. A rapid classification method of aluminum alloy based on laser-induced breakdown spectroscopy and random forest algorithm. Plasma Science and Technology 2019;21. doi: 10.1088/2058-6272/aaf7bf.

[27] Dai Y, Song C, Gao X, Chen A, Hao Z, Lin J. Quantitative determination of Al–Cu–Mg–Fe–Ni aluminum alloy using laser-induced breakdown spectroscopy combined with LASSO–LSSVM regression. Journal of Analytical Atomic Spectrometry 2021;63:1629-1634. doi: 10.1002/mop.32810.

[28] Dai Y, Zhao S, Song C, Gao X. Identification of aluminum alloy by laser-induced breakdown spectroscopy combined with machine algorithm. Microwave and Optical Technology Letters 2021;63:1629-1634. doi: 10.1002/mop.32810.

[29] Menking-Hoggatt K, Arroyo L, Curran J, Trejos T. Novel LIBS method for micro-spatial chemical analysis of inorganic gunshot residues. Journal of Chemometrics 2019;35. doi: 10.1002/cem.3208.